İSTANBUL UNIVERSITY CERRAHPAŞA

ORIGINAL ARTICLE
Electrica 2024; 24(3): 693-709

Modeling of Dual Inverter-Fed Split-Phase Interior Permanent Magnet Synchronous Machine for Electric Vehicle Traction Application

Izuchukwu Nnanna Eze, Linus Uchechukwu Anih, Cosmas Uchenna Ogbuka

Department of Electrical Engineering, University of Nigeria, Nsukka, Enugu State, Nigeria

Cite this article as: I. N. Eze, L. U. Anih, and C. U. Ogbuka, "Modeling of dual inverter-fed split-phase interior permanent magnet synchronous machine for electric vehicle traction application," *Electrica*, 24(3), 693-709, 2024.

ABSTRACT

The quest for efficient, stable, and reliable operation of power devices for electric vehicle traction has intensified over the years for improved performance. To this end, the study on dual inverter-fed split-phase Interior Permanent Magnet Synchronous Machine (IPMSM) is undertaken in order to authenticate the precise magnetic coupling between the split-phase stator winding sets and also to draw inferences on the improved performance characteristics of the machine over their traditional three-phase counterparts. This paper presents a unique and precise circuit representation of IPMSM with the inclusion of mutual slot leakage coupling inductance between the split-phase stator windings energized by two independent space vector pulse width modulated inverters for full utilization of the limited dc battery bank voltage so that the machine can run at rated volts per hertz value in order to sustain the rated load torque without the machine windings being overheated and also to prevent derating. The dynamic and steady-state equivalent circuits are derived in a unique manner. This configuration has high reliability, high torque and power densities, good efficiency, power supply security, and fault tolerance than traditional three-phase PMSM counterparts. The amplitude of current loading and stress in this scheme is 50% less than their three-phase counterparts as the current is shared between the split-phase IPMSM stator winding sets, thereby making the machine thermally stable and robust. Moreover, the current Total Harmonic Distortion (THD) spectrum, speed, and torque ripples of this scheme are also lower than their three-phase counterparts. This configuration shows that the reduction in the current THD spectrum, torque, and speed ripples are 3.19%, 18.16%, and 38.89% respectively, compared to their three-phase counterparts. The results obtained in this split-phase IPMSM by *q-d* and steady-state analyses are remarkably in good agreement. MATLAB software simulation study proves the efficacy of this configuration.

***Index Terms*—**Dual inverters, electric vehicle, load angle, phase shift, space vector modulator, split-phase

I. INTRODUCTION

The groundbreaking development of the internal combustion engine vehicle is one of the greatest advancements of contemporary technology. The concern over the depletion of limited global fossil fuels (coal, petroleum, and natural gas) has motivated and pressurized regulatory bodies and researchers to search for alternative means of transportation traction systems. Besides the health and environmental hazard implications caused by fossil fuels, such as the depletion of the ozone layer, global warming, and urban air and noise pollution, global fossil fuels are depreciating and diminishing over the years due to their over-dependence for energy production and utilization and also for their enormous application in the internal combustion engines of automobiles, aircraft engines, marine engines, and locomotive engines. The search for safe and clean energy has necessitated research for electric vehicle (EV) propulsion systems. Fuel cell vehicles, EVs, and hybrid electric vehicles (HEVs) have been proposed by regulatory bodies and scholars to be close substitutes for typical automobile vehicles in the near future as the globe is tilting toward green energy devoid of environmental pollution and associated health challenges [1].

A. Literature Review

Electric traction systems these days are gaining more attention since they are regarded as the most promising solution to ease the global transportation energy crisis, pollution, and global warming posed by internal combustion engines of automobiles, locomotive engines, aircraft engines, and marine engines. Electric motors, as one of the key devices, determine the main performance of the electric transport system. The first generation of EVs was developed with DC machines, but eventually, the industrial acceptance of AC machines dominated DC machines for EV propulsion [2]. Both Permanent Magnet Synchronous Machine (PMSM) and Induction

Corresponding author:
Izuchukwu Nnanna Eze

E-mail:
izuchukwu.eze.pg02117@unn.edu.ng

Received: October 16, 2023

Revision Requested: August 17, 2024

Last Revision Received: August 23, 2024

Accepted: September 17, 2024

Publication Date: November 8, 2024

DOI: 10.5152/electrica.2024.23131

Machine (IM)-based electric powertrains are being manufactured for EVs and HEVs. Currently, the most common type of electric machine used in the manufacturing of HEVs and EVs is Interior Permanent Magnet Synchronous Machine (IPMSM) [2]. The permanent magnets of IPMSM are embedded inside the rotor structure, which necessitate rotor saliency in this machine. This leads to the development of reluctance torque that enables the machine to operate over a wide range of speed at constant power due to its ability to overcome the flux-weakening phenomenon during electric drive operation while Surface Permanent Magnet Synchronous Machine (SPMSM) has its permanent magnet mounted peripherally on the rotor surface. Rotor saliency and the concomitant reluctance torque do not exist in this case. This drawback limits the application of SPMSM for EV propulsion.

Permanent Magnet Synchronous Machine has high efficiency, high power, and torque densities than IM because, conventionally, the rotor circuit structure has no winding but only a permanent magnet. Multiphase machines have been recognized to possess higher efficiency and reliability than their traditional three-phase counterparts. Besides, they have inherent greater fault tolerance, reduced torque ripple and minimized power electronic rating, which pose a big problem in high drive power applications like EV [3]. The replacement of the field winding of a typical synchronous machine with a permanent magnet results in a machine called PMSM. The DC field excitation is generated by a permanent magnet embedded interiorly or peripherally mounted on the rotor structure. This machine configuration eliminates traditional brushes, slip rings, and the associated field winding copper losses [4]. Due to the absence of rotor cage winding, the machine is not self-starting; hence there exists line-start PMSMs [5]. Due to their non-self-starting nature, they are mostly applied in variable speed drives that require inverters for power supply [6]. The incorporation of split-phase winding into one stator periphery is an improved technology instead of using two electric motors mechanically coupled together since both configurations develop an equal amount of electromagnetic torque [7]. The split-phase IPMSM configuration has higher torque density, higher power density, higher efficiency, fault tolerance, and can be operated over a wide range of speeds at constant power during drive operation within the limited DC bus voltage constraints compared to their three-phase counterparts [8, 9]. This split-phase machine has six sets of stator windings. There are cases where the stator six windings are phase-shifted 30 electrical degrees [8-12], while others are phase-shifted zero electrical degrees [13, 14].

B. Research Gap and Motivation

Having reviewed the literature of related studies, it is discovered that no research has been conducted on dual inverter-fed split-phase IPMSM for EV propulsion with a view to guaranteeing power supply security, fault tolerance, and reliability over their three-phase counterparts. This paper presents a split-phase interior PMSM energized by two independent modulated inverters using the Space Vector Pulse Width Modulation (SVPWM) technique. The scheme is envisaged to have high efficiency, high torque and power densities, reliability, and fault tolerance by guaranteeing power supply security to the machine in the event of failure. This configuration is compared with the configuration when the system is under fault occurrence; that is, when there is a failure in one of the inverters, a DC bus failure of an inverter or a stator winding set failure. These fault phenomena are simply called unhealthy conditions in this paper. The performance characteristics of an inverter-fed typical three-phase IPMSM gave the same results as when this configuration is under an unhealthy state or fault condition. The motivating factor behind this study is embedded in designing a configuration that will be efficient, stable, reliable, and fault tolerant for the propulsion of EVs.

C. Challenges and Limitation of the Research

The drawbacks of this configuration are that a DC bus failure has the likelihood to shut down the machine operation since the inputs of the dual inverters are connected to a common DC bus and also the additional stator winding will invariably necessitate deeper slots, increased slot leakage inductance, and the attendant additional cost. The limitation of this study is that the configuration is not conducted and controlled under any electric motor drive algorithm but is just inverter-fed. Applying any electric motor drive algorithm like direct torque control, field-oriented control, *V*/*F* control, and so on to this configuration is outside the scope of this study.

D. The Contributions of the Research

In the course of the study of this configuration, the major contributions of this research article are

1. The amplitude of current consumed by the split-phase IPMSM stator winding sets is half of that of their typical three-phase counterparts, thereby making the machine thermally stable and robust.
2. There is a reduction in the current Total Harmonic Distortion (THD) spectrum, speed, and torque ripples compared to their three-phase counterparts.
3. The configuration guarantees power supply security and fault tolerance compared to their three-phase counterparts.
4. This configuration also exhibits enhanced performance characteristics in terms of output power, torque, and efficiency compared to their three-phase counterparts.
5. The adoption of the SVPWM technique guarantees the full utilization of the available DC bus battery bank voltage signal, which has advantages over the pulse-width modulation strategy.

II. ELECTROMECHANICAL MODELING OF SPLIT-PHASE IPMSM

The proposed electric motor configuration has two three-phase winding sets wound on the same stator, and equal voltages from the two inverters are supplied to the two sets of polyphase stator winding sets, *abc* and *xyz*, also known as split-phase winding, which are equal in magnitude and direction. The split-phase stator winding angular displacement or stator winding phase shift, ξ, is zero. The assumptions established in this scheme are that the iron losses are ignored, and the sets of the stator split-phase windings are sinusoidally and symmetrically distributed along the air gap. The distributed windings of the split-phase IPMSM have the same number of poles, accommodated in the same stator slots, and share the same magnetic circuit structure. Thus, the split-phase IPMSM are coupled magnetically but electrically isolated. Since split-phase IPMSM share common stator slots, there exists mutual slot coupling leakage inductance. The topology is shown in Fig. 1.

A. The Dynamic Modeling of Split-Phase IPMSM

The dual three-phase stator winding voltage equations of the split-phase IPMSM in state variable form can be respectively expressed as:

$$\begin{cases} V_{ABCS} = r_{abcs} i_{ABCS} + \rho\lambda_{ABCS} \\ V'_{XYZS} = r'_{xyzs} i'_{XYZS} + \rho\lambda'_{XYZS} \end{cases} \quad (1)$$

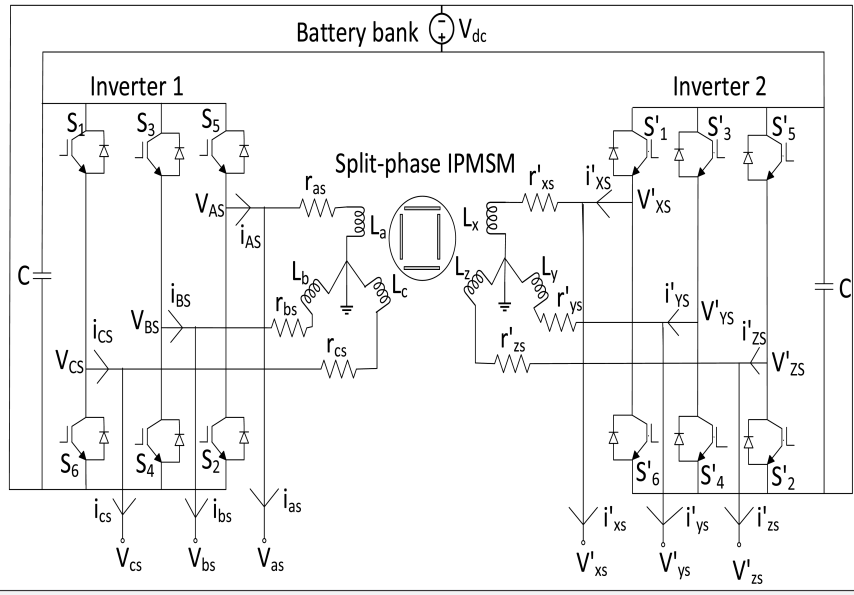

Fig. 1. The topology of the dual inverter-fed split-phase IPMSM.

where, $V_{ABCS} = V_{AS}\, V_{BS}\, V_{CS}{}^{T}, V'_{XYZ} = V'_{XS}\, V'_{YS}\, V'_{ZS}{}^{T}$, $i_{ABCS} = i_{AS}\, i_{BS}\, i_{CS}{}^{T}$, $i'_{XYZS} = i'_{XS}\, i'_{YS}\, i'_{ZS}{}^{T}$, $r_{abcs} = diag\left[r_{as}\, r_{bs}\, r_{cs}\right], r'_{xyz} = diag\left[r'_{xs}\, r'_{ys}\, r'_{zs}\right]$ V_{ABCS} are the three-phase or line voltages across the *abc* winding, V'_{XYZS} are the three-phase voltages across the *xyz* winding referred to the *abc* winding, i_{ABCS} are the 3-phase currents drawn by *abc* winding, i'_{XYZS} are the 3-phase currents drawn by the *xyz* winding referred to the *abc* winding, r_{abcs} are the winding *abc* resistance, r'_{xyz} are the winding *xyz* resistance referred to the *abc* winding, and *T* is the transpose matrix. The per-phase currents, i_{abcs} and i'_{xyzs} are respectively equal to line currents, i_{ABCS} and i'_{XYZS} since the machine is star connected. The dual inverters have a common DC bus voltage, V_{dc}. The dual line voltages are represented as V_{AS}, V_{BS}, V_{CS} for inverter 1 and $V'_{XS}, V'_{YS}, V'_{ZS}$ for inverter 2, while the dual per-phase voltages are also represented as V_{as}, V_{bs}, V_{cs} for inverter 1 and $V'_{xs}, V'_{ys}, V'_{zs}$ for inverter 2, as also shown in Fig. 1.

The change of variables that formulates the transformation of the two three-phase variables of stationary circuit elements to the arbitrary reference coordinates can be written as [4, 15]:

$$\begin{cases} f_{qdo1} = K_s f_{ABCS} \\ f'_{qdo2} = K_s \xi f'_{XYZS} \end{cases} \tag{2}$$

f can be a representation of current, voltage, or flux linkage and the established Robert H. Park transformation equation, K_s is written as [15]:

$$K_s = \frac{2}{3}\begin{bmatrix} cos\theta_r & cos\left(\theta_r - \frac{2\pi}{3}\right) & cos\left(\theta_r + \frac{2\pi}{3}\right) \\ sin\theta_r & sin\left(\theta_r - \frac{2\pi}{3}\right) & sin\left(\theta_r + \frac{2\pi}{3}\right) \\ \frac{1}{2} & \frac{1}{2} & \frac{1}{2} \end{bmatrix}$$

The angular position and velocity of an arbitrary reference coordinate as:

$$\omega_r = d\theta_r / dt \tag{3}$$

The inverse Robert H. Park transformation equation is:

$$\left(K_s\right)^{-1} = \begin{bmatrix} cos\theta_r & sin\theta_r & 1 \\ cos\left(\theta_r - \frac{2\pi}{3}\right) & sin\left(\theta_r - \frac{2\pi}{3}\right) & 1 \\ cos\left(\theta_r + \frac{2\pi}{3}\right) & sin\left(\theta_r + \frac{2\pi}{3}\right) & 1 \end{bmatrix} \tag{4}$$

The split-winding stator winding resistances are equal in every respect; hence, $r_{abcs} = r_{s1}$ for winding set *abc* while $r'_{xyz} = r'_{s2}$ for winding set *xyz* referred to *abc* winding. Applying Park's transformation equation to (1), the voltage equation in the rotor reference coordinate with $\omega = \omega_r$ for V_{ABCS} yields:

$$\begin{cases} V^r_{q1} = r_{s1} i^r_{q1} + \omega_r \lambda^r_{d1} + \rho\lambda^r_{q1} \\ V^r_{d1} = r_{s1} i^r_{d1} - \omega_r \lambda^r_{q1} + \rho\lambda^r_{d1} \\ V^r_{o1} = r_{s1} i^r_{o1} + \rho\lambda^r_{o1} \end{cases} \tag{5}$$

In the same vein, Robert H. Park transformation is also applied to (4) V'_{XYZS} with the incorporation of stator winding arbitrary displacement angle, ξ, and written as:

$$K_s\xi = \frac{2}{3}\begin{bmatrix} cos\left(\theta_r - \xi\right) & cos\left(\theta_r - \xi - \frac{2\pi}{3}\right) & cos\left(\theta_r - \xi + \frac{2\pi}{3}\right) \\ sin\left(\theta_r - \xi\right) & sin\left(\theta_r - \xi - \frac{2\pi}{3}\right) & sin\left(\theta_r - \xi + \frac{2\pi}{3}\right) \\ \frac{1}{2} & \frac{1}{2} & \frac{1}{2} \end{bmatrix} \tag{6}$$

The inverse Park's transformation equation is:

$$\left(K_s\xi\right)^{-1}=\begin{bmatrix} cos\left(\theta_r-\xi\right) & sin\theta_r & 1 \\ cos\left(\theta_r-\xi-\frac{2\pi}{3}\right) & sin\left(\theta_r-\xi-\frac{2\pi}{3}\right) & 1 \\ cos\left(\theta_r-\xi+\frac{2\pi}{3}\right) & sin\left(\theta_r-\xi+\frac{2\pi}{3}\right) & 1 \end{bmatrix} \quad (7)$$

Applying Park's transformation equation to (1), the voltage equation in the rotor reference coordinate

With $\omega=\omega_r$ for $V_{XYZS}^{'}$ yields:

$$\begin{cases} V_{q2}^{'r}=r_{s2}^{'}i_{q2}^{'r}+\omega_r\lambda_{d2}^{'r}+\rho\lambda_{q2}^{'r} \\ V_{d2}^{'r}=r_{s2}^{'}i_{d2}^{'r}-\omega_r\lambda_{q2}^{'r}+\rho\lambda_{d2}^{'r} \\ V_{o2}^{'r}=r_{s2}^{'}i_{o2}^{'r}+\rho\lambda_{o2}^{'r} \end{cases} \quad (8)$$

The armature winding inductances put forward by [8, 9, 16] are:

$$L_{abc}=\begin{bmatrix} L_{aa} & L_{ab} & L_{ac} \\ L_{ba} & L_{bb} & L_{bc} \\ L_{ca} & L_{cb} & L_{cc} \end{bmatrix}=$$

$$\begin{bmatrix} L_{ls1}+L_{a1}-L_{b1}cos2\theta r & -\frac{1}{2}L_{a1}-L_{b1}cos\left(2\theta r-\frac{2\pi}{3}\right) & \dots \\ -\frac{1}{2}L_{a1}-L_{b1}cos\left(2\theta r-\frac{2\pi}{3}\right) & L_{ls1}+L_{a1}-L_{b1}cos2\left(\theta r-\frac{2\pi}{3}\right) & \dots \\ -\frac{1}{2}L_{a1}-L_{b1}cos\left(2\theta r+\frac{2\pi}{3}\right) & -\frac{1}{2}L_{a1}-L_{b}cos2\left(\theta r+\pi\right) & \dots \\ \dots-\frac{1}{2}L_{a1}-L_{b1}cos\left(2\theta r+\frac{2\pi}{3}\right) & & \\ \dots-\frac{1}{2}L_{a1}-L_{b1}cos2\left(\theta r+\pi\right) & & \\ \dots L_{ls1}+L_{a1}-L_{b1}cos\left(2\theta r+\frac{2\pi}{3}\right) & & \end{bmatrix} \quad (9)$$

Where L_{abc} is the self-inductance of the first set of the split-phase winding, *abc*. The self-inductance, L_{xyz} of the second split-phase winding set, *xyz* is:

$$L_{xyz}=\begin{bmatrix} L_{xx} & L_{xy} & L_{xz} \\ L_{yx} & L_{yy} & L_{yz} \\ L_{zx} & L_{zy} & L_{zz} \end{bmatrix}=$$

$$\begin{bmatrix} L_{ls2}+L_{x1}-L_{y1}cos\left(2\theta r-2\xi\right) & -\frac{1}{2}L_{x1}-L_{y1}cos\left(2\theta r-2\xi-\frac{2\pi}{3}\right) & \dots \\ -\frac{1}{2}L_{x1}-L_{y1}cos\left(2\theta r-2\xi-\frac{2\pi}{3}\right) & L_{ls2}+L_{x1}-L_{y1}cos2\left(\theta r-\xi-\frac{2\pi}{3}\right) & \dots \\ -\frac{1}{2}L_{x1}-L_{y1}cos\left(2\theta r-2\xi+\frac{2\pi}{3}\right) & -\frac{1}{2}L_{x1}-L_{y1}cos2\left(\theta r-\xi+\pi\right) & \dots \\ \dots-\frac{1}{2}L_{x1}-L_{y1}cos\left(2\theta r-2\xi+\frac{2\pi}{3}\right) & & \\ \dots-\frac{1}{2}L_{x1}-L_{y1}cos2\left(\theta r-\xi+\pi\right) & & \\ \dots L_{ls2}+L_{x1}-L_{y1}cos\left(2\theta r-2\xi+\frac{2\pi}{3}\right) & & \end{bmatrix} \quad (10)$$

The mutual inductance between the split-phase stator windings is:

$$L_{AX}=\begin{bmatrix} L_{ax} & L_{ay} & L_{az} \\ L_{bx} & L_{by} & L_{bz} \\ L_{cx} & L_{cy} & L_{cz} \end{bmatrix}=$$

$$\begin{bmatrix} L_{a2}cos\xi-L_{b2}cos\left(2\theta r-\xi\right) & L_{a2}cos\left(\xi+\frac{2\pi}{3}\right)-L_{b2}cos\left(2\theta r-\xi-\frac{2\pi}{3}\right) & \dots \\ L_{a2}cos\left(\xi-\frac{2\pi}{3}\right)-L_{b2}cos\left(2\theta r-\xi-\frac{2\pi}{3}\right) & L_{a2}cos\xi-L_{b2}cos\left(2\theta r-\xi+\frac{2\pi}{3}\right) & \dots \\ L_{a2}cos\left(\xi+\frac{2\pi}{3}\right)-L_{b2}cos\left(2\theta r-\xi+\frac{2\pi}{3}\right) & L_{a2}cos\left(\xi-\frac{2\pi}{3}\right)-L_{b2}cos\left(2\theta r-\xi\right) & \dots \\ \dots L_{a2}cos\left(\xi-\frac{2\pi}{3}\right)-L_{b2}cos\left(2\theta r-\xi+\frac{2\pi}{3}\right) & & \\ \dots L_{a2}cos\left(\xi-\frac{2\pi}{3}\right)-L_{b2}cos\left(2\theta r-\xi\right) & & \\ \dots L_{a2}cos\xi-L_{b2}cos\left(2\theta r-\xi-\frac{2\pi}{3}\right) & & \end{bmatrix} \quad (11)$$

Mutual slot-leakage inductance matrix is:

$$L_{l12}=\begin{bmatrix} L_{lax} & L_{lay} & L_{laz} \\ L_{lbx} & L_{lby} & L_{lbz} \\ L_{lcx} & L_{lcy} & L_{lcz} \end{bmatrix} \quad (12)$$

Transforming the inductances to *q – d* reference frames in order to eliminate time-varying inductance yields the stator flux linkage in a compact matrix form as:

$$\begin{bmatrix} \lambda_{qdo1}^{r} \\ \lambda_{qdo2}^{'r} \end{bmatrix}=\begin{bmatrix} K_sL_{abc}\left(K_s\right)^{-1} & L_{abcxyz(qdo)} \\ L_{abcxyz(qdo)} & K_s\xi L_{xyz}\left(K_s\xi\right)^{-1} \end{bmatrix}\begin{bmatrix} i_{qdo1}^{r} \\ i_{qdo2}^{'r} \end{bmatrix}+\lambda_m^{'r}\begin{bmatrix} 0 \\ 1 \\ 0 \end{bmatrix} \quad (13)$$

$$L_{abcxyz(qdo)}=K_sL_{l12}\left(K_s\xi\right)^{-1}+K_sL_{AX}\left(K_s\xi\right)^{-1} \quad (14)$$

$$where\,K_sL_{l12}\left(K_s\xi\right)^{-1}=\begin{bmatrix} L_{lm}^{'} & -L_{lqd} & 0 \\ L_{lqd} & L_{lm}^{'} & 0 \\ 0 & 0 & L_{lax}+L_{lay}+L_{laz} \end{bmatrix},$$

$$K_sL_{AX}\left(K_s\xi\right)^{-1}=\begin{bmatrix} L_{mq} & 0 & 0 \\ 0 & L_{md} & 0 \\ 0 & 0 & 0 \end{bmatrix},K_sL_{abc}\left(K_s\right)^{-1}=\begin{bmatrix} L_q & 0 & 0 \\ 0 & L_d & 0 \\ 0 & 0 & L_{ls1} \end{bmatrix},$$

$$K_s\xi L_{xyz}\left(K_s\xi\right)^{-1}=\begin{bmatrix} L_q & 0 & 0 \\ 0 & L_d & 0 \\ 0 & 0 & L_{ls2}^{'} \end{bmatrix}$$

The stator flux linkage equations of the machine in simplified matrix form are:

$$\begin{bmatrix} \lambda_{q1}^{r} \\ \lambda_{d1}^{r} \\ \lambda_{o1} \end{bmatrix}=\begin{bmatrix} L_q & 0 & 0 \\ 0 & L_d & 0 \\ 0 & 0 & L_{ls1} \end{bmatrix}\begin{bmatrix} i_{q1}^{r} \\ i_{d1}^{r} \\ i_{o1} \end{bmatrix}+\begin{bmatrix} L_{lm}^{'}+L_{mq} & -L_{lqd}^{'} & 0 \\ L_{lqd}^{'} & L_{lm}^{'}+L_{md} & 0 \\ 0 & 0 & L_{lax}+L_{lay}+L_{laz} \end{bmatrix}\begin{bmatrix} i_{q2}^{'r} \\ i_{d2}^{'r} \\ i_{o2} \end{bmatrix}+\lambda_m^{'r}\begin{bmatrix} 0 \\ 1 \\ 0 \end{bmatrix} \quad (15)$$

$$\begin{bmatrix} \lambda_{q2}^{'r} \\ \lambda_{d2}^{'r} \\ \lambda_{o2} \end{bmatrix}=\begin{bmatrix} L_{lm}^{'}+L_{mq} & -L_{lqd}^{'} & 0 \\ L_{lqd}^{'} & L_{lm}^{'}+L_{md} & 0 \\ 0 & 0 & L_{lax}+L_{lay}+L_{laz} \end{bmatrix}\begin{bmatrix} i_{q1}^{'r} \\ i_{d1}^{'r} \\ i_{o1} \end{bmatrix}+\begin{bmatrix} L_q & 0 & 0 \\ 0 & L_d & 0 \\ 0 & 0 & L_{ls2}^{'} \end{bmatrix}\begin{bmatrix} i_{q2}^{'r} \\ i_{d2}^{'r} \\ i_{o2} \end{bmatrix}+\lambda_m^{'r}\begin{bmatrix} 0 \\ 1 \\ 0 \end{bmatrix} \quad (16)$$

where $L'_{lm} = L_{lax}cos\xi + L_{lay}\cos\left(\xi + \frac{2\pi}{3}\right) + L_{laz}\cos\left(\xi - \frac{2\pi}{3}\right)$ denotes common mutual leakage inductance, $L'_{lqd} = L_{lax}sin\xi + L_{lay}\sin\left(\xi + \frac{2\pi}{3}\right) + L_{laz}\sin\left(\xi - \frac{2\pi}{3}\right)$ denotes the cross-mutual coupling inductance between the *d and q* axes of the stator windings, and $\lambda'^{r}_{m} = L_{md}i'_{m}; i'_{m}$ is the equivalent magnetizing current of the rotor permanent referred to the stator side. It is worthy to note that $L_q = L_{ls1} + L_{mq}$ *and* $L_{ls1} = L_{l1} + L'_{lm}$ and $L_d = L_{ls1} + L_{md}$ and $L_{ls1} = L_{l1} + L'_{lm}$. The same principle is applicable to the second winding set. The summary of the flux linkage equations using (15)–(16) considering $L'_{lqd} = 0$ [17] because the arbitrary winding angular displacement, ξ, is zero or split-phase stator windings are phase-shifted zero electrical degree is:

$$\begin{cases} \lambda^{r}_{q1} = L_q i^{r}_{q1} + L'_{lm} i'^{r}_{q2} + L_{mq} i'^{r}_{q2} \\ \lambda^{r}_{d1} = L_d i^{r}_{d1} + L'_{lm} i'^{r}_{d2} + L_{md} i'^{r}_{d2} + \lambda'^{r}_{m} \\ \lambda'^{r}_{q2} = L_q i'^{r}_{q2} + L'_{lm} i^{r}_{q1} + L_{mq} i^{r}_{q1} \\ \lambda'^{r}_{d2} = L_d i'^{r}_{d2} + L'_{lm} i^{r}_{d1} + L_{md} i^{r}_{d1} + \lambda'^{r}_{m} \end{cases} \quad (17)$$

The common mutual leakage inductance L'_{lm} accounts for the mutual coupling due to the leakage flux between stator split-phase windings occupying the same stator slot. It depends on the winding angular displacement between the stator split-phase winding sets and pitch and has a significant impact on the harmonic coupling between them. However, ignoring this parameter has no significant effect on the transient state, except for some changes in voltage harmonic distortion [18]. If L'_{lm} is neglected in the system, (17) can be simplified for the sake of formulating the equivalent circuit and rewritten as:

$$\begin{cases} \lambda^{r}_{q1} = L_{ls1} i^{r}_{q1} + L_{mq}\left(i^{r}_{q1} + i'^{r}_{q2}\right) \\ \lambda^{r}_{d1} = L_{ls1} i^{r}_{d1} + L_{md}\left(i^{r}_{d1} + i'^{r}_{d2}\right) + \lambda'^{r}_{m} \\ \lambda'^{r}_{q2} = L'_{ls2} i'^{r}_{q2} + L_{mq}\left(i^{r}_{q1} + i'^{r}_{q2}\right) \\ \lambda'^{r}_{q2} = L'_{ls2} i'^{r}_{q2} + L_{mq}\left(i^{r}_{q1} + i'^{r}_{q2}\right) \end{cases} \quad (18)$$

The parameters L_d, L_q, L_{md}, L_{mq} are the direct axis inductance, quadrature axis inductance, direct axis mutual inductance, and quadrature axis mutual inductance, respectively. Combining (5), (8), and (18) appropriately results in the dynamic equivalent circuit of the model; hence the equations:

$$\begin{cases} V^{r}_{q1} = r_{s1} i^{r}_{q1} + \omega_r \lambda^{r}_{d1} + \rho\left(L_{ls1} i^{r}_{q1} + L_{mq}\left(i^{r}_{q1} + i'^{r}_{q2}\right)\right) \\ V^{r}_{d1} = r_{s1} i^{r}_{d1} - \omega_r \lambda^{r}_{q1} + \rho\left(L_{ls1} i^{r}_{d1} + L_{md}\left(i^{r}_{d1} + i'^{r}_{d2}\right) + \lambda'^{r}_{m}\right) \\ V'^{r}_{q2} = r'_{s2} i'^{r}_{q2} + \omega_r \lambda'^{r}_{d2} + \rho\left(L'_{ls2} i'^{r}_{q2} + L_{mq}\left(i^{r}_{q1} + i'^{r}_{q2}\right)\right) \\ V'^{r}_{d2} = r'_{s2} i'^{r}_{d2} - \omega_r \lambda'^{r}_{q2} + \rho\left(L'_{ls2} i'^{r}_{d2} + L_{md}\left(i^{r}_{d1} + i'^{r}_{d2}\right) + \lambda'^{r}_{m}\right) \end{cases} \quad (19)$$

Fig. 2a and 2b suggest the dynamic state equivalent circuits appropriately coined from (19).

For a balanced three-phase system, the zero-sequence components of currents and voltages are equal to zero [8, 9].

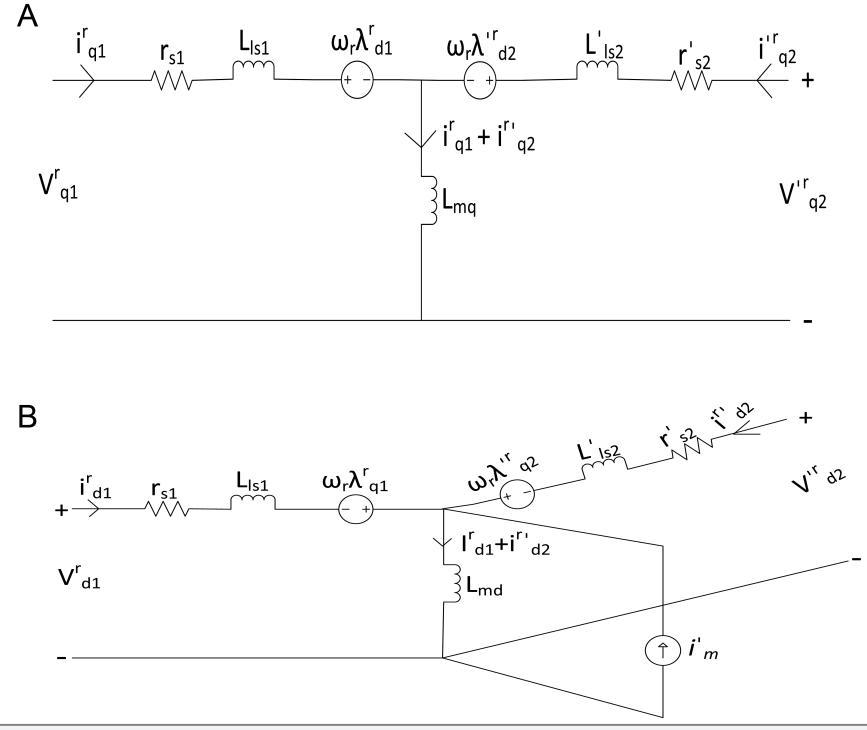

Fig. 2. (a) *q-axis* equivalent circuit (b) *d-axis* equivalent circuit.

B. Development of Dynamic Electromagnetic Torque
The total input power into the machine is given by:

$$P_{in} = V_{AS}i_{AS} + V_{BS}i_{BS} + V_{CS}i_{CS} + V'_{XS}i'_{XS} + V'_{YS}i'_{YS} + V'_{ZS}i'_{ZS} \tag{20}$$

In *qdo* term the input power is given as:

$$P_{in} = \frac{3}{2}\left(V^r_{q1}i^r_{q1} + V^r_{d1}i^r_{d1} + 2V_{o1}i_{o1} + V'^r_{q2}i'^r_{q2} + V'^r_{d2}i'^r_{d2} + 2V_{o2}i_{o2}\right) \tag{21}$$

Substitution of (5), (8), and (17) into (21) yields:

$$P_{in} = \frac{3}{2}\begin{bmatrix} \left(i^{r2}_{q1}r_{s1} + i^{r2}_{d1}r_{s1} + 2i^2_{o1}r_{s1} + i^{r2}_{q2}r'_{s2} + i^{r2}_{d2}r'_{s2} + 2i^2_{o2}r_{s2}\right) \\ +\left(\rho\lambda^r_{q1}i^r_{q1} + \rho\lambda^r_{d1}i^r_{d1} + \rho\lambda'_{q2}i'^r_{q2} + \rho\lambda'^r_{d2}i^{r2}_{d2}\right) \\ +\left(\omega_r\lambda^r_{d1}i^r_{q1} - \omega_r\lambda^r_{q1}i^r_{d1} + \omega_r\lambda'^r_{d2}i'^r_{q2} - \omega_r\lambda'^r_{q2}i'^r_{d2}\right) \end{bmatrix} \tag{22}$$

The first term represents the *Ohmic* losses, the second term represents the rate of change of exchange of magnetic field energy between the split-phase stator windings, while the third term represents the rate of energy conversion to mechanical work. Electromagnetic torque, T_e is:

$$T_e = \frac{3}{2}\frac{\omega_r}{\omega_m}\left(\lambda^r_{d1}i^r_{q1} - \lambda^r_{q1}i^r_{d1} + \lambda'^r_{d2}i'^r_{q2} - \lambda'^r_{q2}i'^r_{d2}\right) \tag{23}$$

$$\frac{p}{2}\omega_m = \omega_r\,\Delta\omega_m = \frac{2}{p}\omega_r \tag{24}$$

where ω_m is the mechanical speed. Substituting (24) into (23) yields:

$$T_e = \frac{3}{2}\frac{p}{2}\left(\lambda^r_{d1}i^r_{q1} - \lambda^r_{q1}i^r_{d1} + \lambda'^r_{d2}i'^r_{q2} - \lambda'^r_{q2}i'^r_{d2}\right) \tag{25}$$

Substituting (17) into (25) yields:

$$T_e = \frac{3}{2}\frac{p}{2}\begin{pmatrix} \left(L_d - L_q\right)i^r_{q1}i^r_{d1} + \left(L_d - L_q\right)i'^r_{q2}i'^r_{d2} \\ +\left(L_{md} - L_{mq}\right)i^r_{q1}i'^r_{d2} + \left(L_{md} - L_{mq}\right)i'^r_{q2}i^r_{d1} \\ +\lambda'^r_m\left(i^r_{q1} + i'^r_{q2}\right) \end{pmatrix} \tag{26}$$

The result of this derived electromagnetic equation shows that L'_{lm} does not contribute to the torque development and therefore can be neglected in the model as stated earlier. The first component of (26) represents reluctance torque developed due to stator winding *abc*, the second component represents the reluctance torque developed due to stator winding *xyz*, the third and fourth components represent torque developed due to interaction between stator windings *abc* and *xyz*, while the fifth component represents excitation torque developed from the field of the embedded permanent magnet. The equations describing the mechanical parts of the split-phase machine are:

$$\begin{cases} \dfrac{d\omega_r}{dt} = \dfrac{P}{2J}\left(T_e - \dfrac{2B_m}{P}\omega_r - T_L\right) \\ \dfrac{d\theta_r}{dt} = \omega_r \end{cases} \tag{27}$$

TABLE I. SPLIT-PHASE INTERIOR PERMANENT MAGNET SYNCHRONOUS MOTOR PARAMETERS

Rated power (KW)	20
Rated speed (rpm)	1500
Number of poles	4
Stator resistance (Ohm)	0.45
L_d, *d* – axis inductance (mH)	6
L_q, *q* – axis inductance (mH)	16.9
moment of inertia (kg.m^2)	0.01
Viscous friction coefficient (N.m.s/rad)	0.01
Permanent magnet flux (Wb)	0.51
L_{ls}, stator winding leakage inductance (mH)	1.00
dc bus voltage (V)	500

Where B_m, J, p, and T_L are the viscous friction coefficient, moment of inertia, number of poles of the machine, and load torque, respectively. The parameters of the machine are given in Table I [9].

C. The Dynamic Modeling Differential Equations of the Machine
A precise machine model is essential since the machine behavior depends on the mathematical equations describing it. Since the machine windings are symmetrical, it is assumed that $i^r_{q1} = i'^r_{q2}$ *and* $i^r_{d1} = i'^r_{d2}$. Besides (27), other differential equations describing the dynamic modeling of the machine using equations (5), (8), and (18) in state-space form noting that $\rho\lambda'^r_m = 0$ are:

$$\rho i^r_{q1} = \frac{V^r_{q1} - r_{s1}i^r_{q1} - \omega_r\left(L_d + L_{md}\right)i^r_{d1} - \omega_r\lambda'^r_m}{\left(L_q + L_{mq}\right)} \tag{28}$$

$$\rho i^r_{d1} = \frac{V^r_{d1} - r_{s1}i^r_{d1} + \omega_r\left(L_q + L_{mq}\right)i^r_{q1}}{\left(L_d + L_{md}\right)} \tag{29}$$

$$\rho i'^r_{q2} = \frac{V'^r_{q2} - r'_{s2}i'^r_{q2} - \omega_r\left(L_d + L_{md}\right)i'^r_{d2} - \omega_r\lambda'^r_m}{\left(L_q + L_{mq}\right)} \tag{30}$$

$$\rho i'^r_{d2} = \frac{V'^r_{d2} - r'_{s2}i'^r_{d2} + \omega_r\left(L_q + L_{mq}\right)i'^r_{q2}}{\left(L_d + L_{md}\right)} \tag{31}$$

The derivatives of the stator flux linkages can be written in state-space form as:

$$\rho\lambda^r_{q1} = V^r_{q1} - r_{s1}i^r_{q1} - \omega_r\left(L_d + L_{md}\right)i^r_{d1} - \omega_r\lambda'^r_m \tag{32}$$

$$\rho\lambda^r_{d1} = V^r_{d1} - r_{s1}i^r_{d1} + \omega_r\left(L_q + L_{mq}\right)i^r_{q1} \tag{33}$$

$$\rho\lambda'^r_{q2} = V'^r_{q2} - r'_{s2}i'^r_{q2} - \omega_r\left(L_d + L_{md}\right)i'^r_{d2} - \omega_r\lambda'^r_m \tag{34}$$

$$\rho\lambda'^r_{d2} = V'^r_{d2} - r'_{s2}i'^r_{d2} + \omega_r\left(L_q + L_{mq}\right)i'^r_{q2} \tag{35}$$

III. THE INVERTER-FED SPLIT-PHASE IPMSM USING SPACE VECTOR MODULATOR

Due to the non-self-starting characteristics of the split-phase IPMSM [6], it is energized with two independent inverters of the same rating using Space Vector Modulator (SVM). The maximum possible per-phase output voltage of the carrier-based pulse width modulation technique is limited to $0.5V_{dc}$, while the maximum possible line-to-line output voltage of the carrier-based pulse width modulation technique is limited to $\sqrt{3}/2V_{dc}$ [19]. The main drawback with the three-phase carrier-based pulse width modulation inverter concepts is the minimized peak fundamental output line-to-line voltage $\sqrt{3}V_{dc}$ that can be achieved compared to the available and limited DC bus voltage. This drawback has important implications for motor drive applications, where it is very desirable to use a rated voltage in variable speed motor drive applications [20]. In SVM, the relationship that constrains the peak possible magnitude of output per-phase voltage, V_o is [20]:

$$V_o = \frac{2\sqrt{3}}{3}V_{dc} = \frac{2}{\sqrt{3}}V_{dc} \tag{36}$$

while the peak possible *line–to–line* output voltage using SVM must equal [15]:

$$V_{l-l} = \sqrt{3}V_o = 2V_{dc} \tag{37}$$

This analysis shows that a 15% increase in modulation index can be achieved using SVM. With this full utilization of DC bus voltage, the dual three-phase SVM inverter-fed split-phase IPMSM can now run at rated load torque without derating. A summary of merits of SVM technique over carrier-based pulse width modulation is given in reference [21]. The operation of top and bottom switches is complementary. The split-phase IPMSM stator voltage vectors expressed in the stationary reference coordinate can be secured by using the appropriate switching states and the common DC link bus voltage, *Vdc*, as:

$$\begin{cases} V_{abcs} = 2/3V_{dc}\left(S_a + aS_b + a^2S_c\right) \\ V'_{xyzs} = 2/3V_{dc}\left(S'_x + aS'_y + a^2S'_z\right) \end{cases} \tag{38}$$

$a = j2\pi/3$. A simple proof of (38) can be obtained as an explicit consequence of the physical fact that the split-phase IPMSM stator line voltages can be written as:

$$\begin{cases} V_{ABS} = V_{AS} = V_{dc}\left(S_a - S_b\right) \\ V_{BCS} = V_{BS} = V_{dc}\left(S_b - S_c\right) \\ V_{CAS} = V_{CS} = V_{dc}\left(S_c - S_a\right) \\ V'_{XYS} = V'_{XS} = V_{dc}\left(S'_x - S'_y\right) \\ V'_{YZS} = V'_{YS} = V_{dc}\left(S'_y - S'_z\right) \\ V'_{ZXS} = V'_{ZS} = V_{dc}\left(S'_z - S'_x\right) \end{cases} \tag{39}$$

Howbeit, the split-phase IPMSM stator per-phase voltages can be obtained from (39) as:

$$\begin{cases} V_{as} = 1/3\left(V_{ABS} - V_{CAS}\right) \\ V_{bs} = 1/3\left(V_{BCS} - V_{ABS}\right) \\ V_{cs} = 1/3\left(V_{CAS} - V_{BCS}\right) \\ V'_{xs} = 1/3\left(V'_{XYS} - V'_{ZXS}\right) \\ V'_{ys} = 1/3\left(V'_{YZS} - V'_{XYS}\right) \\ V'_{zs} = 1/3\left(V'_{ZXS} - V'_{YZS}\right) \end{cases} \tag{40}$$

Substituting the expressions of the stator line voltages into the stator per-phase voltages gives:

$$\begin{cases} V_{as} = V_{dc}/3\left(2S_a - S_b - S_c\right) \\ V_{bs} = V_{dc}/3\left(2S_b - S_a - S_c\right) \\ V_{cs} = V_{dc}/3\left(2S_c - S_a - S_b\right) \\ V'_{xs} = V_{dc}/3\left(2S'_x - S'_y - S'_z\right) \\ V'_{ys} = V_{dc}/3\left(2S'_y - S'_x - S'_z\right) \\ V'_{zs} = V_{dc}/3\left(2S'_z - S'_x - S'_y\right) \end{cases} \tag{41}$$

This two identical dual three-phase SVM method of (41) is utilized to generate gate pulses for the dual three-phase voltage source inverters powering the split-phase IPMSM. Considering the split-phase IPMSM stator per-phase voltages, the stator space voltage vectors are:

$$\begin{cases} V_{abcs} = 2/3\left(V_{as} + V_{bs}e^{j\left(2/3\right)\pi} + V_{cs}e^{j\left(4/3\right)\pi}\right) \\ V'_{xyzs} = 2/3\left(V'_{xs} + V'_{ys}e^{j\left(2/3\right)\pi} + V'_{zs}e^{j\left(4/3\right)\pi}\right) \end{cases} \tag{42}$$

The primary line voltages are determined by the status of the switches of the identical dual inverters. Therefore, there are eight voltage space vectors each for the dual inverters, which are:

$\overline{V_1}(100), \overline{V_2}(110), \overline{V_3}(010), \overline{V_4}(011), \overline{V_5}(001) and \overline{V_6}(101)$ for active voltage space vectors while $\overline{V_0}(000) and \overline{V_7}(111)$ for the zero voltage space vectors. Here, 0 represents that the bottom switch is "OFF" while 1 represents that the top switch is "ON." Switching ON the inverter switches in any given legs $\left(S_a, S_b or S_c\right)$ and $\left(S_x, S_y or S_z\right)$ will short the circuit and therefore should not be attempted. The inverters are controlled in such a manner that in a given leg of the dual identical inverters, either the top switch $\left(S_1, S_3 or S_5\right)$ is ON and the bottom switch $\left(S_4, S_6 or S_2\right)$ is OFF or vice versa for inverter 1; similarly for inverter 2, either the top switch $\left(S'_1, S'_3 or S'_5\right)$ is ON and the bottom switch $\left(S'_4, S'_6 or S'_2\right)$ is OFF or vice versa. The inverter 1 switching variables for the first switching state can summarily be defined as:

$$S_a = \begin{cases} 0 if\ S_1 is OFF\ and\ S_4 is ON \\ 1 f\ S_1 is ON\ and\ S_4 is OFF \end{cases} \tag{43}$$

$$S_b = \begin{cases} 0 if\ S_3\ is\ OFF\ and\ S_6\ is\ ON \\ 1 if\ S_3\ is\ ON\ and\ S_6\ is\ OFF \end{cases} \quad (44)$$

$$S_c = \begin{cases} 0 if\ S_5\ is\ OFF\ and\ S_2\ is\ ON \\ 1 if\ S_5\ is\ ON\ and\ S_2\ is\ OFF \end{cases} \quad (45)$$

while the inverter 2 switching variables for the first switching state can also be summarily defined as:

$$S_x = \begin{cases} 0 if\ S_1^{'}\ is OFF\ and\ S_4^{'}\ is ON \\ 1 if\ S_1^{'}\ is ON\ and\ S_4^{'}\ is OFF \end{cases} \quad (46)$$

$$S_y = \begin{cases} 0 if\ S_3^{'}\ is OFF\ and\ S_6^{'}\ is ON \\ 1 if\ S_3^{'}\ is ON\ and\ S_6^{'}\ is OFF \end{cases} \quad (47)$$

$$S_z = \begin{cases} 0 if\ S_5^{'}\ is OFF\ and\ S_2^{'}\ is ON \\ 1 if\ S_5^{'}\ is ON\ and\ S_2^{'}\ is OFF \end{cases} \quad (48)$$

Fig. 3 shows the switching pattern, and the values of the switching functions are also represented together with the exact switching positions.

A. Dynamic Simulation of Split-Phase IPMSM

The machine under this study is not a line-start IPMSM but an inverter-fed IPMSM. The machine is simulated using MATLAB. The battery bank DC bus voltage is 500 V_{dc}. The model is conducted under the over-modulation range by virtue of SVM. The results are shown in Fig. 4a to 7g.

IV. STEADY-STATE ANALYSIS OF THE SPLIT-PHASE IPMSM

If $r_{s1} = r_{s2}^{'} = r_s = 0$ and the frictional and windage losses are neglected, then the electrical power into the machine equals the mechanical output power of the machine [22], hence:

$$P_s = \left(\frac{2}{p}\right)\omega_r T_e \quad (49)$$

Where ω_r is the synchronous speed. At steady-state, all the differential terms are equated to zero. The balanced instantaneous power into the split-phase IPMSM is:

$$P_s = \frac{3}{2}\left(V_{q1}^r I_{q1}^r + V_{d1}^r I_{d1}^r + V_{q2}^{'r} I_{q2}^{'r} + V_{d2}^{'r} I_{d2}^{'r}\right) \quad (50)$$

In the rotor reference coordinate, the stator $q-d$ voltages become constant voltages:

$$\begin{cases} V_{q1}^r = V_{as} cos\delta \\ V_{d1}^r = -V_{as} sin\delta \\ V_{q2}^{'r} = V_{xs}^{'} cos\left(\delta - \xi\right) \\ V_{d2}^{'r} = -V_{xs}^{'} sin\left(\delta - \xi\right) \end{cases} \quad (51)$$

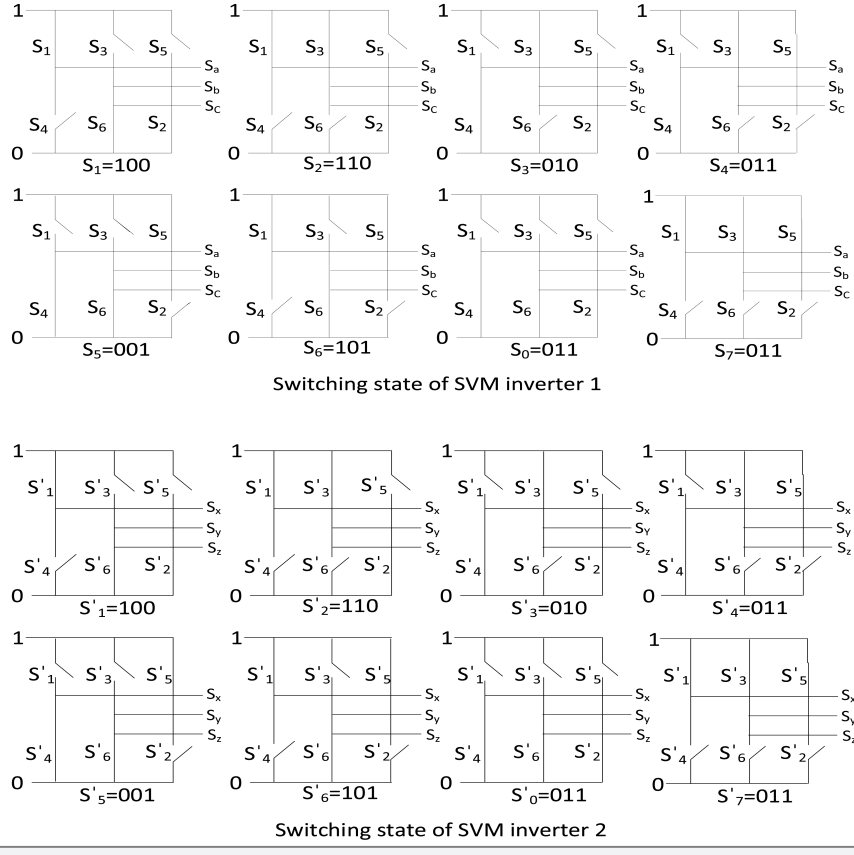

Fig. 3. The dual inverters switching patterns.

$$\begin{cases} V_{q1}^{r} = \omega_r \left(L_d I_{d1} + L_{md} I_{d2} + \lambda_m^{r} \right) = X_d I_{d1} + X_{md} I_{d2} + E_{pm} \\ V_{d1}^{r} = -\omega_r \left(L_q I_{q1} + L_{md} I_{q2} \right) = -X_q I_{q1} - X_{mq} I_{q2} \\ V_{q2}^{r} = \omega_r \left(L_d I_{d2} + L_{md} I_{d1} + \lambda_m^{r} \right) = X_d I_{d2} + X_{md} I_{d1} + E_{pm} \\ V_{d2}^{r} = -\omega_r \left(L_q I_{q2} + L_{md} I_{q1} \right) = -X_q I_{q2} - X_{mq} I_{q1} \end{cases} \tag{52}$$

where $\omega_r \lambda_m^{r} = \omega_r L_{md} i_m^{'} = E_{pm}$. If rs_1 and $r_{s2}^{'}$ are by far less than the reactances, solving for $I_{q1}^{r}, I_{d1}^{r}, I_{q2}^{'r}$ and $i_{d2}^{'r}$ from (51) and (52) yields:

$$\begin{cases} I_{q1}^{r} = \dfrac{-\left(V_{as} X_q \sin\delta - V_{xs}^{'} X_{mq} \sin\left(\delta - \xi\right) \right)}{X_{mq}^2 - X_q^2} \\ I_{d1}^{r} = \dfrac{-\left(E_{pm} X_d - E_{pm} X_{md} + V_{xs}^{'} X_{md} \cos\left(\delta - \xi\right) - V_{as} X_d \cos\delta \right)}{X_d^2 - X_{md}^2} \\ I_{q2}^{'r} = \dfrac{\left(V_{as} X_{mq} \sin\delta - V_{xs}^{'} X_q \sin\left(\delta - \xi\right) \right)}{X_{mq}^2 - X_q^2} \\ I_{d2}^{'r} = \dfrac{-\left(E_{pm} X_d - E_{pm} X_{md} - V_{xs}^{'} X_d \cos\left(\delta - \xi\right) + V_{as} X_{md} \cos\delta \right)}{X_d^2 - X_{md}^2} \end{cases} \tag{53}$$

The magnitudes of the split-phase per-phase stator currents are:

$$\begin{cases} I_{as} = \sqrt{I_{q1}^{2} + I_{d1}^{2}} \\ I_{xs}^{'} = \sqrt{I_{q2}^{'r2} + I_{d2}^{'r2}} \end{cases} \tag{54}$$

while the magnitudes of the split-phase per-phase stator voltages are:

$$\begin{cases} V_{as} = \sqrt{V_{q1}^{r2} + V_{d1}^{r2}} \\ V_{xs}^{'} = \sqrt{V_{q2}^{'r2} + V_{d2}^{'r2}} \end{cases} \tag{55}$$

Substituting (51) and (53) into the power equation of (50) and simplifying yields:

$$P_s = \frac{3}{2} \left(\begin{array}{l} \dfrac{\left(V_{as} E_{pm} X_d \sin\delta - V_{as} E_{pm} X_{md} \sin\delta + V_{xs}^{'} E_{pm} X_d \sin\left(\delta - \xi\right) - V_{xs}^{'} E_{pm} X_{md} \sin\left(\delta - \xi\right) \right)}{X_d^2 - X_{md}^2} + \\ \dfrac{\left(V_{as} V_{xsX_{md}}^{'} \sin\delta \cos\left(\delta - \xi\right) - V_{as}^2 X_d \cos\delta \sin\delta - V_{xs}^{'2} X_d \cos\left(\delta - \xi\right) \sin\left(\delta - \xi\right) + V_{as} V_{xsX_{md}}^{'} \cos\delta \sin\delta \left(\delta - \xi\right) \right)}{X_d^2 - X_{md}^2} + \\ \dfrac{V_{xs}^{'} \cos\left(\delta - \xi\right) \left(V_{as} X_{mq} \sin\delta - V_{xs}^{'} X_q \sin\left(\delta - \xi\right) \right) - V_{as} \cos\delta \left(V_{as} X_q \sin\delta - V_{xs}^{'} X_{mq} \sin\left(\delta - \xi\right) \right)}{X_{mq}^2 - X_q^2} \end{array} \right) \tag{56}$$

Finding an expression for the steady-state electromagnetic torque from (49) yields:

$$P_s = \left(\frac{2}{p} \right) \omega_r T_e \Rightarrow T_e = \frac{P}{2\omega_r} P_s \tag{57}$$

Substituting (56) into (57) yields:

$$T_e = \frac{3}{2} \cdot \frac{p}{2\omega_r} \left(\begin{array}{l} \dfrac{\left(V_{as} E_{pm} X_d \sin\delta - V_{as} E_{pm} X_{md} \sin\delta + V_{xs}^{'} E_{pm} X_d \sin\left(\delta - \xi\right) - V_{xs}^{'} E_{pm} X_{md} \sin\left(\delta - \xi\right) \right)}{X_d^2 - X_{md}^2} + \\ \dfrac{\left(V_{as} V_{xsX_{md}}^{'} \sin\delta \cos\left(\delta - \xi\right) - V_{as}^2 X_d \cos\delta \sin\delta - V_{xs}^{'2} X_d \cos\left(\delta - \xi\right) \sin\left(\delta - \xi\right) + V_{as} V_{xsX_{md}}^{'} \cos\delta \sin\delta \left(\delta - \xi\right) \right)}{X_d^2 - X_{md}^2} + \\ \dfrac{V_{xs}^{'} \cos\left(\delta - \xi\right) \left(V_{as} X_{mq} \sin\delta - V_{xs}^{'} X_q \sin\left(\delta - \xi\right) \right) - V_{as} \cos\delta \left(V_{as} X_q \sin\delta - V_{xs}^{'} X_{mq} \sin\left(\delta - \xi\right) \right)}{X_{mq}^2 - X_q^2} \end{array} \right) \tag{58}$$

The torque equation of (58) has two components: the first term is the excitation torque, while the second and third terms represent the reluctance torque.

A. The Copper Loss and Efficiency of the Machine

The copper loss due to the split stator windings when the stator winding resistances are equal is:

$$\text{Copper loss, } P_{cu} = 3 r_s \left(\left(I_{q1}^2 + I_{d1}^2 \right) + \left(I_{q2}^{'2} + I_{d2}^{'2} \right) \right) \tag{59}$$

Substituting (53) into (59) yields:

$$P_{cu} = \left(\begin{array}{l} \left(\left(\dfrac{-\left(V_{as} X_q \sin\delta - V_{xs}^{'} X_{mq} \sin\left(\delta - \xi\right) \right)}{X_{mq}^2 - X_q^2} \right)^2 + \left(\dfrac{-\left(E_{pm} X_d - E_{pm} X_{md} + V_{xs}^{'} X_{md} \cos\left(\delta - \xi\right) - V_{as} X_d \cos\delta \right)}{X_d^2 - X_{md}^2} \right)^2 \right) + \\ \left(\left(\dfrac{\left(V_{as} X_{mq} \sin\delta - V_{xs}^{'} X_q \sin\left(\delta - \xi\right) \right)}{X_{mq}^2 - X_q^2} \right)^2 + \dfrac{-\left(E_{pm} X_d - E_{pm} X_{md} - V_{xs}^{'} X_d \cos\left(\delta - \xi\right) + V_{as} X_{md} \cos\delta \right)^2}{X_d^2 - X_{md}^2} \right) \end{array} \right) \tag{60}$$

$$\text{Efficiency of the machine} = \frac{\text{output power}}{\text{input power}} = \frac{\text{Output power}}{\text{output power} + \text{losses}} \tag{61}$$

B. The Steady-State Equivalent Circuit of the Split-Phase IPMSM

At steady state, the derivative terms in (5) and (8) will be zero. Neglecting zero-sequence equation variables, the voltage equations are:

$$\begin{cases} V_{q1}^{r} = r_{s1} I_{q1}^{r} + \omega_r \lambda_{d1}^{r} \\ V_{d1}^{r} = r_{s1} I_{d1}^{r} - \omega_r \lambda_{q1}^{r} \\ V_{q2}^{'r} = r_{s2}^{'} I_{q2}^{'r} + \omega_r \lambda_{d2}^{'r} \\ V_{d2}^{'r} = r_{s2}^{'} I_{d2}^{'r} - \omega_r \lambda_{q2}^{'r} \end{cases} \tag{62}$$

These voltages are related to the synchronously rotating phasors, V_{as} and $V_{xs}^{'}$ as:

$$\begin{cases} V_{as} e^{-j\delta} = V_{q1}^{r} - j V_{d1}^{r} \\ V_{xs}^{'} e^{-j\left(\delta - \xi\right)} = V_{q2}^{'r} - j V_{d2}^{'r} \end{cases} \tag{63}$$

Also, the currents are related to the synchronously rotating phasors, I_{as} and $I_{xs}^{'}$ as:

$$\begin{cases} I_{as} e^{-j\delta} = I_{q1}^{r} - j I_{d1}^{r} \\ I_{xs}^{'} e^{-j\left(\delta - \xi\right)} = I_{q2}^{'r} - j I_{d2}^{'r} \end{cases} \tag{64}$$

Simplifying (62) for V_{q1}^{r} and V_{d1}^{r} and incorporating (17) into it, noting that $L_{lm}^{'}=0$ yields:

$$\begin{cases} V_{q1}^{r}=r_{s1}i_{q1}^{r}+X_{ls1}I_{d1}^{r}+X_{md}I_{d1}^{r}+X_{md}I_{d2}^{'r}+E_{pm} \\ -jV_{d1}=-jr_{s1}i_{d1}^{r}+jX_{ls1}I_{q1}^{r}+jX_{mq}I_{q1}^{r}+jX_{mq}I_{q2}^{'r} \end{cases} \tag{65}$$

Simplifying $V_{q1}^{r}-jV_{d1}^{r}$ from (65) and substituting $i_{q1}^{r}-ji_{d1}^{r}$ from (64) into it yields:

$$V_{q1}^{r}-jV_{d1}^{r}=r_{s1}I_{as}e^{-j\delta}+jX_{ls1}I_{as}e^{-j\delta}+X_{md}\left(I_{d1}^{r}+I_{d2}^{'r}\right)+jX_{mq}\left(I_{q1}^{r}+I_{q2}^{'r}\right)+E_{pm} \tag{66}$$

Recall from (64) that

$$\begin{cases} I_{as}e^{-j\delta}=i_{q1}^{r}-ji_{d1}^{'r}\Rightarrow i_{q1}^{r}=I_{as}e^{-j\delta}+ji_{d1}^{r} \\ I_{xs}e^{-j(\delta-\xi)}=I_{q2}^{'r}-jI_{d2}^{'r}\Rightarrow I_{q2}^{'r}=I_{xs}^{'}e^{-j(\delta-\xi)}+jI_{d2}^{'r} \end{cases} \tag{67}$$

Substituting (67) into (66) by noting that $V_{q1}^{r}-jV_{d1}^{r}=V_{as}e^{-j\delta}$ and solving for V_{as} yields:

$$V_{as}=\frac{V_{q1}-jV_{d1}}{e^{-j\delta}}=\left(r_{s1}+jX_{ls1}\right)I_{as}+X_{md}\left(I_{d1}^{r}+I_{d2}^{'r}\right)e^{j\delta}$$

$$-X_{mq}\left(I_{d1}^{r}+I_{d2}^{'r}\right)e^{j\delta}+jX_{mq}\left(I_{as}+I_{xs}^{'}e^{j\xi}\right)+E_{pm}e^{j\delta}$$

where speed voltage, $E_{a1}=\left(\left(X_{md}-X_{mq}\right)\left(I_{d1}^{r}+I_{d2}^{'r}\right)+E_{pm}\right)e^{j\delta}$

$$V_{as}=\left(r_{s1}+jX_{ls1}\right)I_{as}+jX_{mq}\left(I_{as}+I_{xs}^{'}e^{j\xi}\right)+E_{a1} \tag{68}$$

Simplifying (62) $V_{q2}^{'r}$ and $V_{d2}^{'}$ also incorporating (17) into it, noting that $L_{lm}^{'}=0$ results in:

$$\begin{cases} V_{q2}^{'r}=r_{s2}^{'}I_{q2}^{'r}+X_{ls2}^{'}I_{d2}^{'r}+X_{md}I_{d1}^{r}+X_{md}I_{d2}^{'r}+E_{pm} \\ -jV_{d2}^{'r}=-jr_{s2}^{'}I_{d2}^{'r}+jX_{ls2}^{'}I_{q2}^{'r}+jX_{mq}I_{q1}^{r}+jX_{mq}I_{q2}^{'r} \end{cases} \tag{69}$$

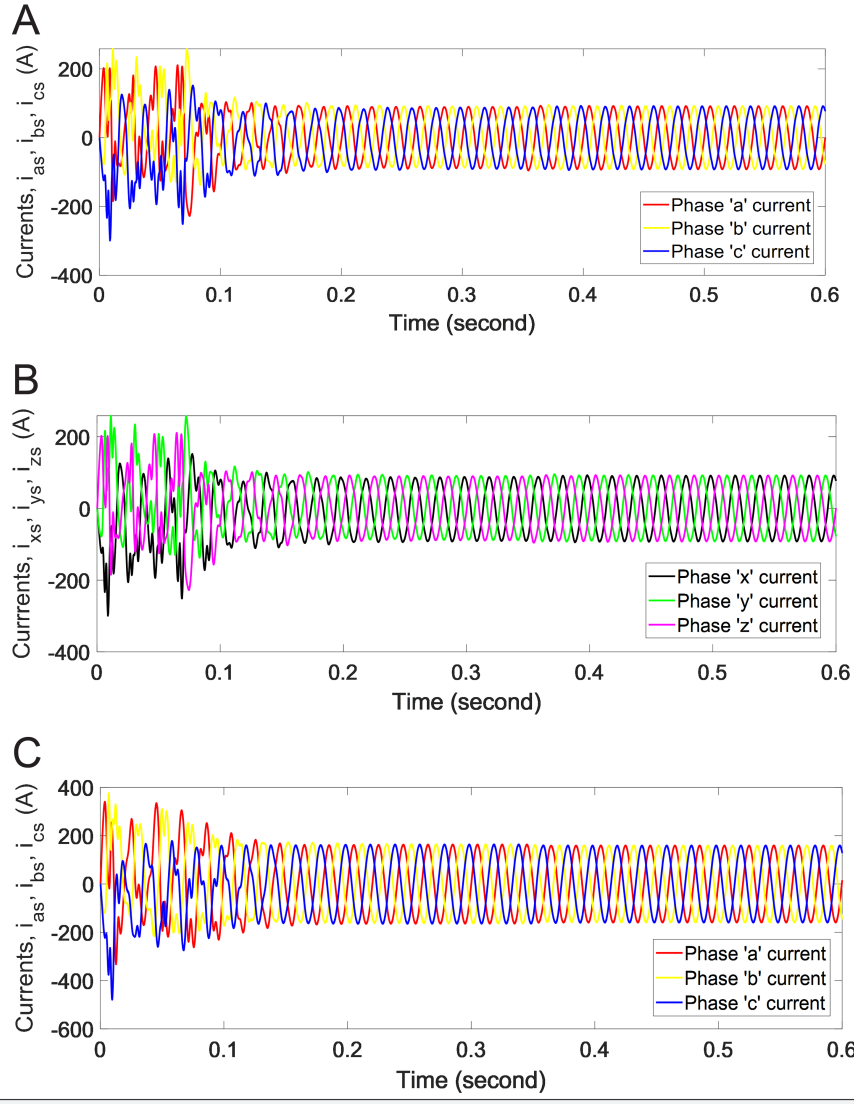

Fig. 4. (a) Stator winding *abc* phase currents during healthy state. (b) Stator winding *xyz* phase currents during healthy state. (c) Stator winding *abc* phase currents during fault condition.

Simplifying $V_{q2}^{'r} - jV_{d2}^{'r}$ from (69) and substituting $I_{q2}^{'r} - jI_{d2}^{'r}$ from (64) into it results in:

$$V_{q2}^{'} - jV_{d2}^{'} = r_{s2}^{'} I_{xs}^{'} e^{-j(\delta-\xi)} + jX_{ls2}^{'} I_{xs}^{'} e^{-j(\delta-\xi)} + X_{md}\left(I_{d1}^{r} + I_{d2}^{'r}\right) + jX_{mq}\left(I_{q1}^{r} + I_{q2}^{'r}\right) + E_{pm} \quad (70)$$

Substituting (67) into (70) by noting that $V_{q2}^{'} - jV_{d2}^{'} = V_{xs}^{'} e^{-j(\delta-\xi)}$ and solving for $V_{x2}^{'}$ yields:

$$V_{xs}^{'} = \frac{V_{d2}^{'} - jV_{d2}^{'}}{e^{-j(\delta-\xi)}} = r_{s2}^{'} I_{xs}^{'} + jX_{ls2}^{'} I_{xs}^{'} + X_{md}\left(I_{d1}^{r} + I_{d2}^{'r}\right) e^{j(\delta-\xi)} - X_{mq}\left(I_{d1}^{r} + I_{d2}^{'r}\right) e^{j(\delta-\xi)} + jX_{mq}\left(I_{as} e^{-j\xi} + I_{xs}^{'}\right) + E_{pm} e^{j(\delta-\xi)} \quad (71)$$

Multiplying (71) by $e^{j\xi}$ yields:

$$V_{xs}^{'} e^{j\xi} = \left(r_{s2}^{'} + jX_{ls2}^{'}\right) I_{xs}^{'} e^{j\xi} + jX_{mq}\left(I_{as} + I_{xs}^{'} e^{j\xi}\right) + E_{a2} \quad (72)$$

where speed voltage, $E_{a2} = X_{md}\left(I_{d1}^{r} + I_{d2}^{'r}\right) e^{j\delta} - X_{mq}\left(I_{d1}^{r} + I_{d2}^{'r}\right) e^{j\delta} + E_{pm} e^{j\delta}$ equal to each other, hence; $E_{a1} = E_{a2} = E_a$ Equations (68) and (72) suggest the steady-state equivalent circuit of the split-phase IPMSM shown in Fig. 8.

The terminal voltages, V_{as} and are taken as the reference phasors in constructing the phasor diagram. The corresponding values of (68) and (72) are used to show it as shown in Fig. 9.

C. Steady-State Simulation of Split-Phase IPMSM

The steady-state simulation of IPMSM is conducted using MATLAB, and the results are shown below. The results are shown in Fig. 10a to 10f.

V. DISCUSSION

The utilized stator line voltage from each of the SVM modulated inverters' output is 1000 V_{ac} as established in (37); that is, the AC line voltage to the machine is *twice* the DC link bus voltage, as evidenced in Fig. 5. With this rated line voltage level, the motor is run at its rated volt per hertz value without derating, which is indispensable in electric motor drives for EV propulsion applications. The dynamic modeling of the inverter-fed split-phase IPMSM is simulated at no-load for 600 ms, and it accelerates to synchronous speed (1500 rpm) with damped oscillations. A load torque of 120 N.m was introduced to it at 350 ms when the machine had overcome oscillations and attained synchronous speed. The machine rotor oscillated briefly and later resettled at synchronous speed, as shown Fig. 6e. Fig. 4a and 4b show the current drawn by the healthy split-phase IPMSM stator winding sets. These currents are equally shared between the windings and are low thereby making the machine thermally stable and robust. The amplitude of the current drawn by the machine under fault condition is *twice* the current drawn by the machine under healthy condition, as shown in Fig. 4c. Since the current waveforms did not show significant oscillation when load was added at 350 ms, more load torques can be tolerated without causing serious perturbation to the dual inverters powering the machine. Different torques developed by the machine include excitation torque, reluctance torque, and torque developed due to interaction between

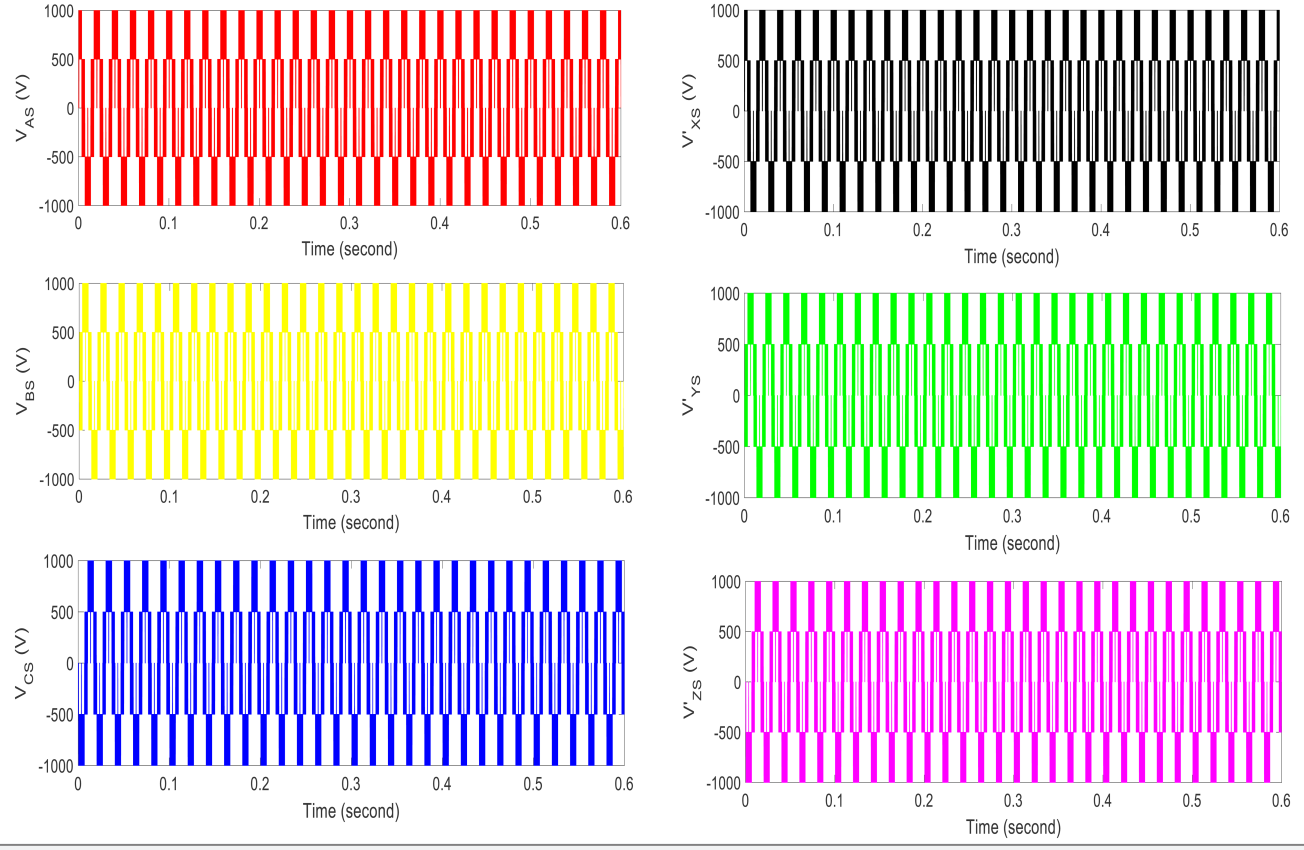

Fig. 5. The dual inverters' line voltages.

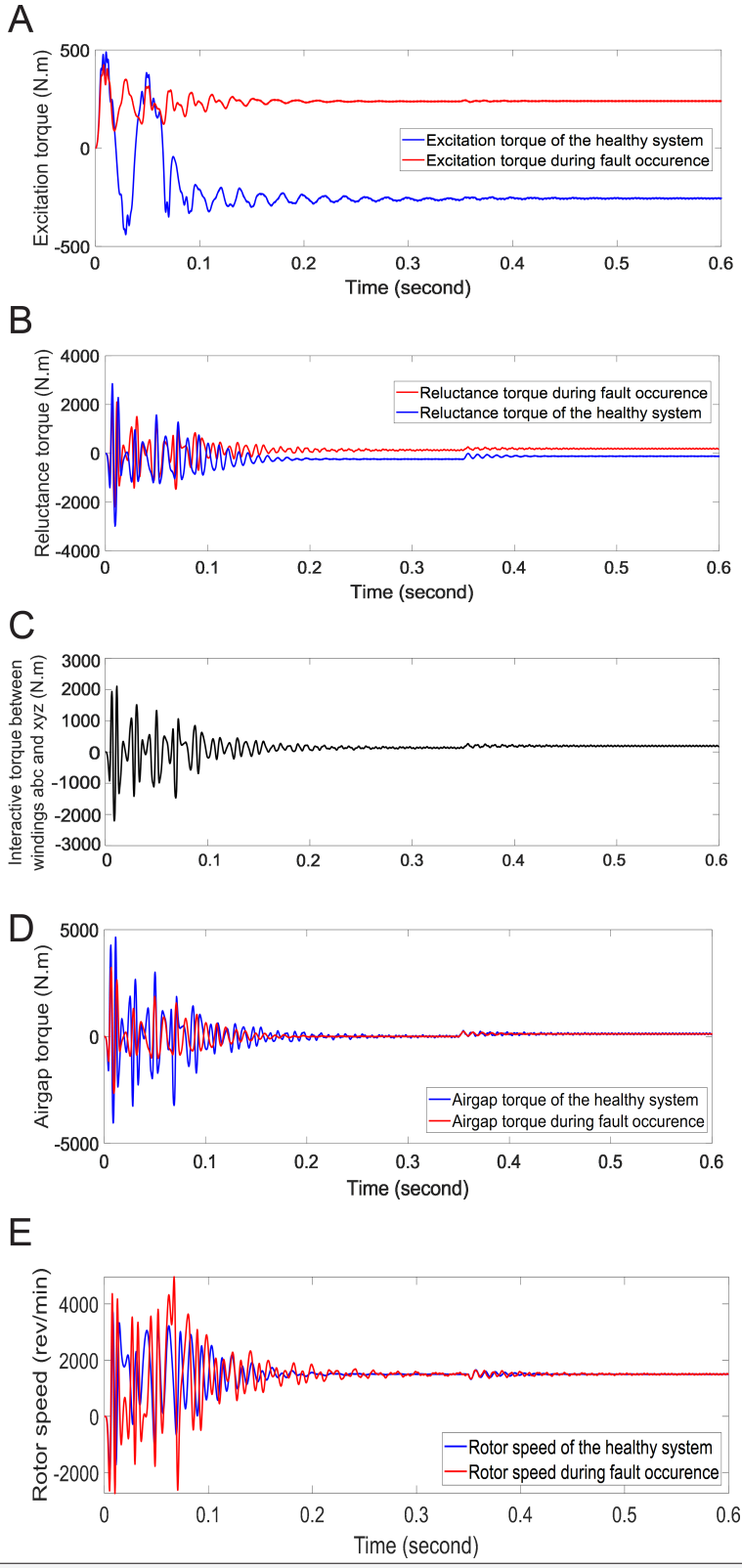

Fig. 6. (a) Excitation torque. (b) Reluctance torque. (c) Interactive torque between stator winding sets *abc and xyz*. (d) Airgap torque. (e). The rotor speed.

the stator winding sets, as shown in Fig. 6a to 6c and summation of these torques yields the airgap/total torque developed by the machine, shown in Fig. 6d, which shows improvement compared to the torque developed by the machine under fault conditions. The development of reluctance torque by the machine due to the rotor pole saliency is responsible for the operation of IPMSM over a wide

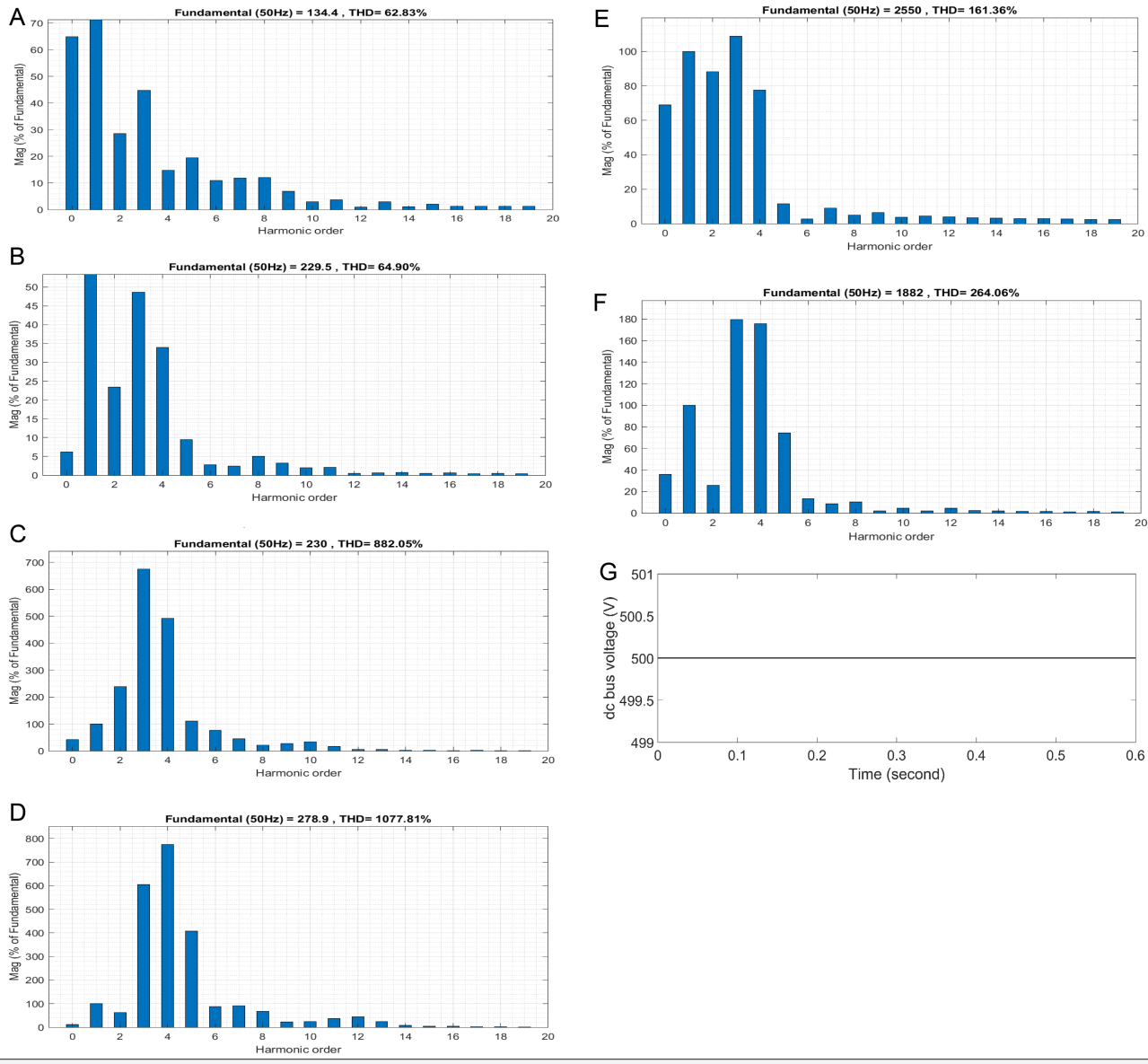

Fig. 7. (a) The current harmonic distortion of the healthy system. (b) The current harmonic distortion of the system under fault condition. (c) The torque ripple of the healthy system. (d) The torque ripple of the unhealthy system. (e) The speed ripple of the healthy system. (f) The speed ripple of the unhealthy system. (g) The DC bus voltage.

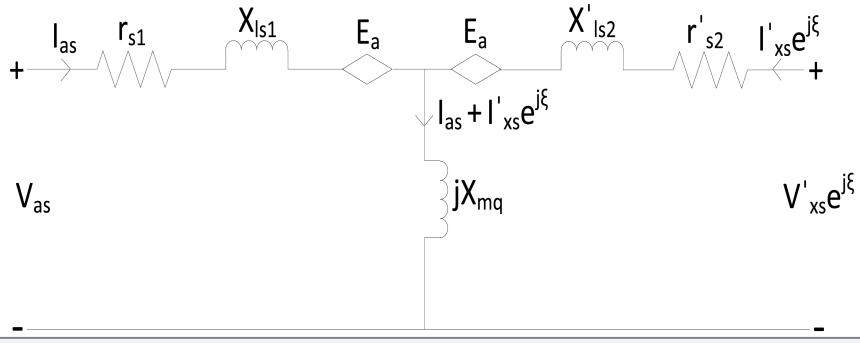

Fig. 8. The per-phase steady-state equivalent circuit of the split-phase IPMSM.

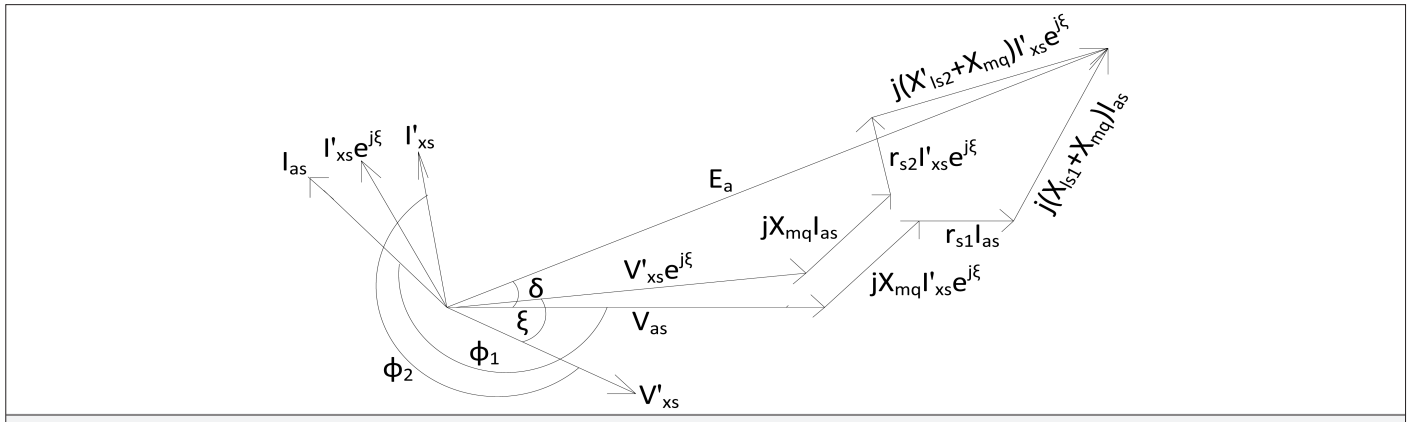

Fig. 9. The per-phase steady-state phasor diagram of the split-phase IPMSM.

speed range of speeds at constant power if the motor is applied in electric drive operations. This phenomenon is beyond the scope of this manuscript. There is a reduction in the current THD spectrum, torque ripple, and speed ripple of the healthy system, while there exists an increase in current THD spectrum, torque ripple, and speed ripple when the system is under fault condition. This configuration shows that a reduction in the current THD spectrum compared to the configuration under fault condition is 3.19%, as deduced respectively from Fig. 7a and 7b. The reduction in torque and speed ripples of the healthy configuration compared to the configuration under fault condition using THD results is 18.16% and 38.89%, respectively, as deduced from Fig. 7c to 7f. The operation of the machine under

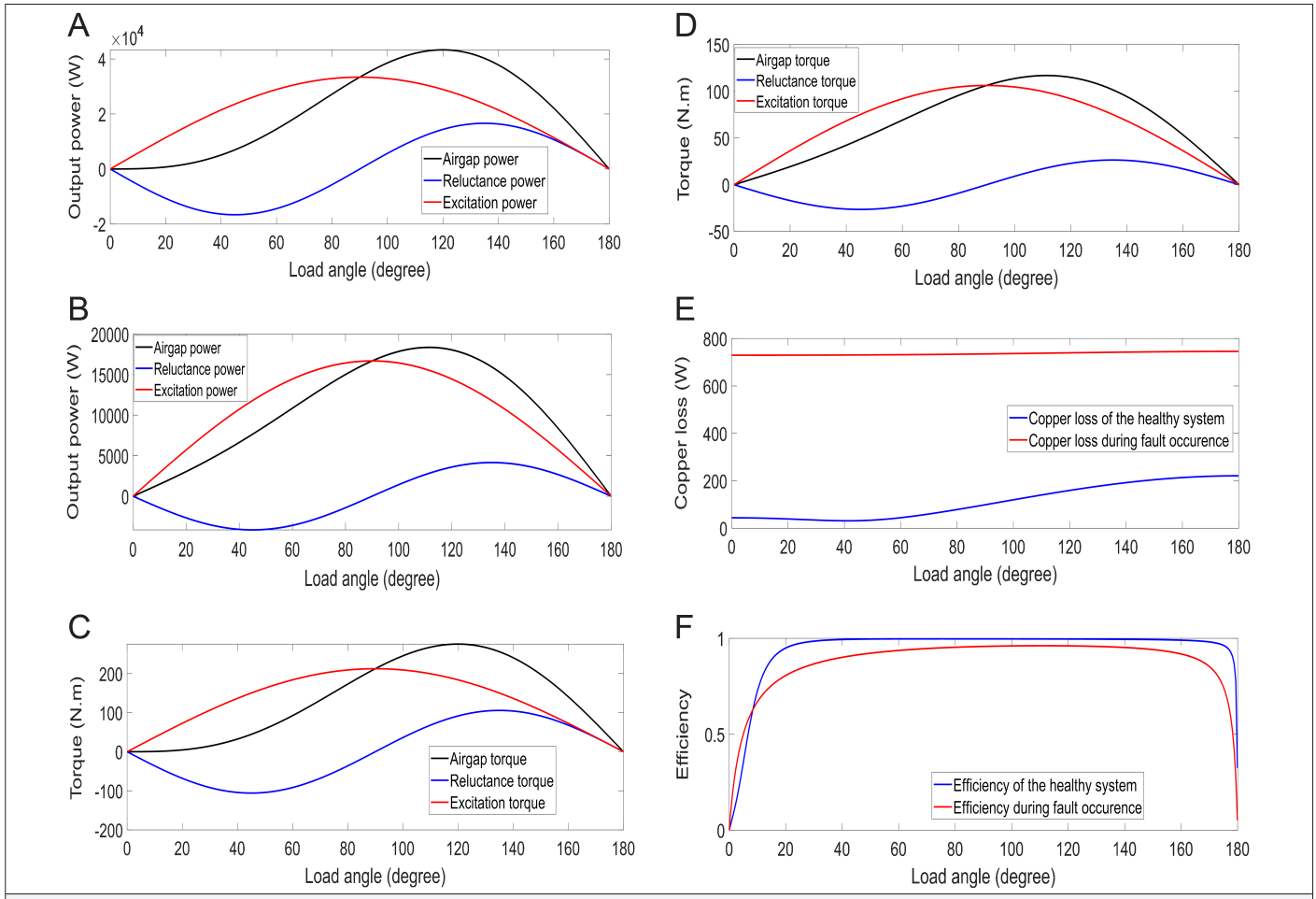

Fig. 10. (a) Steady-state characteristics of output power-load angle of the healthy configuration. (b) Steady-state characteristics of output power-load angle of the unhealthy configuration. (c) Steady-state characteristics of torque-load angle of the healthy configuration. (d) Steady-state characteristics of torque-load angle of the unhealthy scheme. (e) Steady-state characteristics of copper loss-load angle of the healthy and unhealthy conditions. (f) Steady-state characteristics of efficiency–load angle of the healthy and unhealthy conditions.

TABLE II. SUMMARIZED ANALYSIS OF PERFORMANCE CHARACTERISTIC FEATURES OF THE STUDY

The configuration under healthy conditions	The configuration under unhealthy conditions
The current drawn by the machine windings is less and is shared equally between the winding sets, thereby making the machine thermally stable and robust.	The current drawn by a machine winding is high, thereby making the machine thermally unstable and unrobust.
The amplitude of the current drawn by the healthy system is half of the current drawn by the unhealthy system.	The amplitude of the current drawn by the unhealthy system is twice the current drawn by the healthy system.
The efficiency, torque, and power densities are higher.	The efficiency, torque, and power densities are lower.
Power supply security is guaranteed.	Power supply security is not guaranteed.
The configuration has fault tolerance	The configuration does not have fault tolerance
The current harmonic distortion spectrum, torque ripple, and speed ripples are low.	The current harmonic distortion spectrum, torque ripple, and speed ripples are high.
The dc voltage utilization is in obedience to the SVM principle.	The dc voltage utilization is also in obedience to the SVM principle.
The copper loss is low.	The copper loss is very high.

healthy conditions guarantees reliability, excellent efficiency, fault tolerance, and ensures power supply security because a failure of an inverter, or a stator winding set failure, or DCbus failure of an inverter does not tantamount to the shutdown of the entire system. The DC bus voltage is stable and constant throughout the simulation, even when load torque is introduced, as shown in Fig. 7g.

During steady-state operation, the airgap torque is the summation of the developed excitation and reluctance torques. The maximum of this airgap torque is at a load angle greater than 90°, and the reluctance torque component only contributes to this effect by affecting the maximum value of the airgap electromagnetic torque and the load angle at which it occurs. The reluctance electromagnetic torque enhances the airgap torque when the load angle lies within the region of 90° to 180° and minimizes the electromagnetic torque when the load angle lies within the region of 0°–90°. For this reason, the operation of the machine when the load angle lies within 0°–90° is not typically attempted, and the preferred load angle of operation lies affirmatively within the region of 90°–180°. The amplitude of the output power and torque of the healthy system is *twice* their respective output power and torque of the system under fault conditions, as shown in Fig. 10a to 10d. The electrical loss calculation does not include iron and frictional losses. The copper loss in the machine is only contributed by the split-phase stator winding sets since there is no winding in the rotor, but permanent magnet. This leads to an improvement in the efficiency of the machine. The copper loss of the healthy system is very low compared to the system under fault conditions, which is very high, as shown in Fig. 10e. The steady-state efficiency of the healthy split-phase IPMSM when there is no failure of an inverter or a DC bus failure of an inverter is 0.9957, while that of the system under fault condition is 0.9490 over a wide range of load angles shown in Fig. 10f. Besides, the efficiency of the healthy configuration is more stable and covers a wider range of load angles than the efficiency of the fault condition, as also seen in Fig. 10f. From the unique steady-state equivalent circuit of the split-phase IPMSM in Fig. 8, it is observed that two sources of electricity from the dual inverters are fed to the split-phase machine and, moreover, there exists magnetic coupling between the split-phase IPMSM stator winding sets. The derived equivalent circuits are used to predetermine the performance behavior of the machine under different operating conditions. This configuration guarantees reliability and power supply security to the machine when deployed for electric traction drive applications. Fig. 9 shows the drawn phasor diagram of the split-phase machine. Table II shows the summarized performance characteristics of this scheme during both healthy and unhealthy conditions. The performance characteristics of the unhealthy conditions of this configuration gave the same result as that of an inverter-fed typical three-phase IPMSM.

VI. CONCLUSION

The study of the two independent space vector pulse width modulated inverters fed from a common DC bus powering split-phase IPMSM for EV applications is concluded. The machine was operated at the nominal volt per hertz mode with the help of typical SVM dual inverters. This study is conducted without any electric motor drive/control technique, utilizing just inverter fed. From the results of this configuration, it can be deduced that if this configuration is adopted in an electric drive for EV applications and there occurs a failure in a machine winding set or an inverter failure or a DC bus failure of an inverter, the second one can continue to operate without any significant change but an adjustment of the torque command value is needed to be half of the rated value since the machine can no longer by default develop the rated torque. The dynamic analysis is derived with the inclusion of mutual leakage coupling inductance between the split-phase stator winding sets. The results obtained in this split-phase machine by *q-d* and steady-state analyses are in good agreement. This configuration is more cost-effective than mechanically coupling two three-phase IPMSMs together since they develop an equal amount of torque. The significance of this study in a practical environment is that the application of this scheme for EV propulsion will ensure guaranteed power supply security from the dual inverters to the split-phase machine, high efficiency, fault tolerance, and high power and torque densities which are the demerits of the traditional three-phase machine. Moreover, the machine can be operated over a wide speed range of speeds at constant power within the limited DC bus battery bank voltage. Another inherent advantage of this scheme in the practical world is the reduced power electronic component ratings, which constitutes enormous challenges in high-power drive applications [3]. In this respect, the configuration can be adopted as an alternative to electric drive systems using multi-level converters.

Availability of Data and Materials: The data that support the findings of this study are available on request from the corresponding author.

Peer-review: Externally peer-reviewed.

Author Contributions: Concept – I.N.E., L.U.A., C.U.O.; Design – I.N.E., L.U.A., C.U.O.; Supervision – L.U.A., C.U.O.; Resources – I.N.E., L.U.A., C.U.O.; Materials – I.N.E., L.U.A., C.U.O.; Data Collection and/or Processing – I.N.E.; Analysis and/or Interpretation – I.N.E., L.U.A., C.U.O.; Literature Search – I.N.E.; Writing – I.N.E.; Critical Review – L.U.A., I.N.E.

Declaration of Interests: The authors have no conflict of interest to declare.

Funding: The authors declared that this study has received no financial support.

REFERENCES

1. M. Ehsani, Y. Gao, S. E. Gay, and A. Emadi, *Modern Electric, Hybrid Electric and Fuel Cell Vehicles: Fundamentals, Theory and Design*. Boca Raton, FL: CRC Press LLC, 2004.
2. E. Levi, "Multiphase electric machines for variable-speed applications," *IEEE Trans. Ind. Electron.*, vol. 55, no. 5, pp. 1893–1909, 2008. [CrossRef]
3. E. Levi, R. Bojoi, F. Profumo, H. A. Toliyat, and S. Williamson, "Multiphase induction motor drives - A technology status review," *IET Electr. Power Appl.*, vol. 1, no. 4, pp. 489–516, 2007. [CrossRef]
4. P. Krause, O. Wasynczuk, S. Sudhoff, and S. Petarek, *Analysis of Electric Machinery and Drive Systems*, 3rd ed. Hoboken, NJ: John Wiley & Sons, 2013.
5. D. P. M. Cahil, and M. Adkins, "The permanent magnet synchronous motor," *Proc. Instit. Electrical Engineers*, vol. 109, no.48, pp. 483–491, 1962.
6. H. Abu-Rub, A. Iqbal, and J. Guzinski, *High Performance Control of AC Drives with MATLAB/Simulink Models*. Chichester, West Sussex: John Wiley & Sons, 2012.
7. L. Parsa, "On advantages of multi-phase machines," 31st Ann. Conf. IEEE Ind. Electronics Society, Raleigh, North Carolina, Nov. 6–10, 2005. [CrossRef]
8. S. Haghbin, S. Lundmark, M. Alakula, and O. Carlson, "An isolated high-power integrated charger in electrified-vehicle applications," *IEEE Trans. Veh. Technol.*, vol. 60, no. 9, pp. 4115–4126, 2011. [CrossRef]
9. S. Haghbin, T. Torbjorn, and O. Carlson, "An integrated split-phase dual-inverter permanent magnet synchronous motor and battery charger for grid-connected electric or hybrid vehicles," XXth Int. Conf. Electrical Machines, Marseille, France, Sep. 2–5, 2012, 2012.
10. N. Gupta, T. G. Gopika, and R. S. Kaarth, "Modeling and decoupled control of series-connected split-phase synchronous machine with open-circuit fault," *IEEE Trans. Ind. Appl.*, vol. 56, no. 1, pp. 325–334, Jan/Feb. 2019.
11. R. S. Kaarthik, G. R. Srikara, and K. S. Ram, "Decoupled control of series-connected split-phase synchronous motors with open-circuit fault with eight-legged inverter," *IEEE Trans. Transp. Electrif.*, vol. 8, no. 2, pp. 1819–1827, 2022. [CrossRef]
12. Z. Pan, and R. A. Bkayrat, "Modular motor/converter system topology with redundancy for high-speed, high power application," *IEEE Trans. Power Electron.*, vol. 25, no. 2, pp. 408–416, 2010.
13. S. Haghbin, S. Lundmark, O. Carlson, and M. Alakula, "A combined motor/drive/battery charger based on a split-windings PMSM," IEEE Vehicle Power Prop. Conf., Chicago, Illinois, Sept. 6–9, 2011, 2011. [CrossRef]
14. S. V. Nair, P. Harikrishnan, and K. Hatua, "Six-step operation of a symmetric dual three-phase PMSM with minimal circulating currents for extended speed range in electric vehicles," *Ind. Electrons*, IEEE, Trans., vol. 69, no. 8, pp. 7651–7662, 2021.
15. R. H. Park, "Two reaction theory of synchronous machines–generalized method of analysis–part 1," *Trans. Am. Inst. Electr. Eng.*, vol. 48, no.3, pp. 716–727, 1929. [CrossRef]
16. R. F. Schiferl, C. M., and Ong, "Six phase synchronous machine with ac and dc stator connections, Part 1: Equivalent circuit representation and steady-state analysis," *Power Appl. Sys.*, vol, IEEE, Trans., vol. 8. PAS-102, pp. 2685–2693, 1983.
17. O. J. Tola, and E. S. Obe, "ES and L.U. Anih," *Model. Anal. Dual Stator Permanent Magnet Synchronous Mot.* 3rd Int. Conf. Electro-tech. for Nat. Developm. (NIGERCON). IEEE Publications. Owerri, Nigeria, Nov. 7-10, 2017, 2017.
18. A. Igbal, G. K. Singh, and V. Pant, "Steady-state modeling and analysis of six-phase synchronous motor," *Syst. Sci. Control Eng.*, vol. 2, no. 1, pp. 236–249, 2014. [CrossRef]
19. K. Zhou, and D. Wang, "Relationship between space vector modulation and three-phase carrier-based PWM: A comprehensive analysis," *IEEE Trans. Ind. Electron.*, vol. 49, no. 1, pp. 186–196, 2002.
20. D. G. Holmes, and T. A. Lipo, *Pulse Width Modulation for Power Converters: Principles and Practice*. Hoboken, NJ: John Wiley and Sons, 2003.
21. M. H. Rashid, *Power Electronics Handbook*. San Diego, CA: Academic Press, 2001.
22. T. A. Lipo, *Analysis of Synchronous Machine, 2nd Edition*. Boca Raton, FL: CRC Press, 2012.

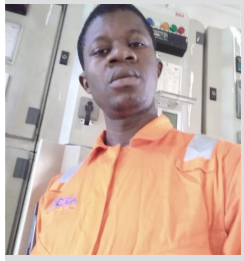

Engr. Izuchukwu Nnanna Eze received B.Eng. and M.Eng. in Electrical Engineering in 2012 and 2016 respectively form University of Nigeria, Nsukka. He is currently pursuing doctorate degree in Electrical Engineering from the same University. He is also a Protection, Control and Metering Engineer at Abuja Electricity Distribution Company, Nigeria. He researches on Power Systems, Electric Machines and Drives.

Linus U. Anih received B.Eng. in Electrical and Electronic Engineering from Anambra State University of Technology, Enugu, Nigeria in 1984, M.Eng. in Electrical and Electronic engineering in 1988 from Obafemi Awolowo University, Ile-Ife, Nigeria and Ph.D. in Electrical Engineering in 1999 from the University of Nigeria, Nsukka. He rose to the rank of Professor in 2009 with specialty in electric machines and drives. He has attended local and international conferences. He has published technical papers in several local and international journals in the field of power systems, electric machines and electric motor drives.

Cosmas U. Ogbuka bagged B.Eng, M.Eng and Ph.D in the Electrical Engineering in the year 2004, 2009, and 2014 respectively from University of Nigeria, Nsukka. He was a postdoctoral fellow at Massachusetts Institute of Technology, MIT, USA, University of Federal Defense, Munich, Germany and University of Valladolid, Spain. He attained electrical engineering professorial position in 2023. He has attended local and international conferences and also published technical papers in local and international journals in the field of electric power devices and control.